Journal of
Renewable Energy Research and Applications (RERA)

Vol. 7, No 1, 2026, 1-10 *DOI: 10.22044/rera.2025.16443.1438*

Design and simulation of a photovoltaic-thermal hybrid system with a spectral filter for enhanced solar energy utilization

Li. Qinghai*, A. Bourhani Said, Yan Yusen, Zhou Hui and Zhang Yanguo

Haidian District Tsinghua University Zijing departement, Beijing, China.

Received Date 20 October 2025; Revised Date 24 December 2025; Accepted Date 24 December 2025
**Corresponding author: liqh@tsinghua.edu.cn (Li. Qinghai)*

Abstract

This study presents the design and simulation of a concentrating photovoltaic-thermal (CPVT) hybrid system that integrates spectral beam splitting (SBS) technology. The system utilizes conventional heliostat mirrors with dual-axis tracking to concentrate sunlight onto both a monocrystalline photovoltaic module and a thermal receiver. $Nb_2O_5/SiO_2/K_9$ spectral filter, with high transmittance in the 580–1100 nm range, is used to separate high-energy photons for photovoltaic conversion and low-energy photons for thermal energy production. The optimal installation position and angle of the mirrors and components were determined, and simulations were conducted to assess the system's performance. The proposed hybrid system achieved a photovoltaic electrical efficiency of 18.00%, a thermal efficiency of 34.29%, and an overall system electrical efficiency of 26.57%. These results highlight the effectiveness of both the spectral filter and the concentration system, positioning this hybrid solution as a promising approach to maximize solar energy utilization.

Keywords: *Concentrating photovoltaic-thermal, Spectral beam splitting, Thermal receiver, Heliostat mirrors, Electrical efficiency.*

1. Introduction

The global dependence on fossil fuels as the main energy source has led to serious en-vironmental problems and the depletion of limited resources [1]. To reduce the harmful effects of climate change and ensure a sustainable energy future, there has been a strong push toward developing and adopting renewable energy technologies. Among these, solar energy is a key solution, as it is abundant, clean, and inexhaustible. Solar energy can be used in various ways, with the most common technologies being photovoltaic (PV) systems and solar thermal systems. Photovoltaic systems directly convert sunlight into electricity using semiconductor materials, making them highly versatile and widely applicable. However, a significant portion of the solar energy absorbed by PV modules is lost as waste heat, which not only reduces efficiency but also accelerates the degradation of PV materials over time. Today's commercial PV systems typically achieve efficiency levels between 15% and 20% for silicon-based cells [2], with the remaining energy dissipated as heat.

On the other hand, solar thermal systems are designed to capture sunlight for heating purposes, which can then be used for applications such as water heating, industrial pro-cesses, and electricity generation through thermodynamic cycles [3]. Solar thermal systems primarily rely on concentrating technologies, including tower, parabolic trough, dish, and linear Fresnel reflector systems, to focus sunlight and generate high temperature heat [4]. While these systems are efficient in capturing and utilizing thermal energy, they cannot directly produce electricity, limiting their standalone use. Additionally, solar thermal systems often require large-scale infrastructure and face challenges related to high operational and maintenance costs, especially in harsh environments.

To address these limitations, photovoltaic-thermal (PV/thermal) hybrid systems have been developed. These systems combine both PV and thermal technologies in one inte-grated system [5]. Traditional PV/thermal systems typically use a cooling mechanism, such as circulating fluid, to remove excess heat from PV modules, keeping them efficient and extending their useful life. Although this approach improves electrical output and system reliability, the thermal energy recovered is usually of low grade, with fluid temperatures staying below 100°C. As a result, these systems are mainly used for low-temperature applications, like residential water heating

Xing Ju et al. [6] created a three-dimensional model of a PV/thermal hybrid system. They combined CFD and TRNSYS methods to explore the effects of different types of solar cells.

Their results showed that with 50 times solar concentration and a flow rate of 0.08 m·s−1, the exergy efficiency followed the order: InGaP/GaAs/InGaAs(37.53%)>GaAs(29.62%)Ga InP (21.62%).

This type of hybrid system aims to optimize the utilization of solar energy by splitting the solar spectrum into two parts: wavelengths that are best suited for photovoltaic con-version and the remaining ones for thermal use[7]. Achieving this requires efficient spectral beam-splitting technologies to separate and direct specific wavelength bands to the PV and CSP subsystems. Several methods have been explored for the implementation of such hy-brid systems, including the use of nanostructured filters, nanofluids, and multijunction solar cells[8, 9, 10]. Among these, spectral beam splitters based on thin-film interference struc-tures have gained prominence due to their precise wavelength selectivity, durability, and compatibility with existing solar technologies. Materials such as perovskite solar cells have also shown potential as integrated components within beam-splitting systems[11], offering tunable optical properties and high efficiency.

In recent years, concentrated photovoltaic-thermal (CPVT) systems have emerged as a more advanced solution for improving the energy conversion efficiency of PV/thermal systems [12, 13, 14]. CPVT systems use optical concentrators, such as parabolic mirrors or Fresnel lenses, to focus sunlight onto PV cells and thermal receivers. This not only reduces the amount of PV cell area needed but also allows the generation of higher-temperature fluids, which broadens the system’s potential applications, including district heating, industrial processes, and thermal power generation. Among the different CPVT configurations, spectral beam splitting (SBS) systems have gained attention for their unique ability to separate solar radiation into distinct wavelength bands [15].

SBS CPVT systems use spectral filters to divide sunlight into high-energy photons for PV electricity generation and low-energy photons for thermal energy production. By separating the thermal and PV components, SBS CPVT systems offer several advantages, such as reducing thermal stress on PV cells and producing high-grade heat that can be used for industrial purposes [16, 17, 18, 19]. Various spectral filtering techniques have been explored, including interference filters, liquid absorptive filters, holographic filters, and nanofluid-based filters. These methods help control the distribution of solar radiation, improving the overall system efficiency [20].

A comprehensive review on concentrating photovoltaic-thermal (CPVT) systems was presented by Jeeja Jacob et al. [21], focusing on applications in clean energy, thermal man-agement strategies, and integration with thermal energy storage. The review summarized commonly employed concentrator structures in CPVT systems, including trough, Fresnel, and parabolic types, along with spectral beam-splitting strategies. Superior performance was highlighted for the combination of short-wave pass filters and multijunction PV modules in enhancing the synergistic efficiency of electrical and thermal energy conversion. Addition-ally, enhanced heat transfer capabilities of nanofluids for thermal module cooling and the application of phase change materials (PCMs) for peak shaving, load leveling, and system stability improvement were emphasized. Diverse application pathways of CPVT systems in building energy supply, seawater desalination, and industrial process heat were discussed. Future developments are suggested to focus on system simplification, material cost reduction, and integrated optimization of intelligent control, aiming to achieve commercial viability and sustainable deployment of CPVT technologies.

While there have been advances in CPVT technology, most existing studies focus on only one aspect of system performance or on theoretical designs. Some research has looked into the impact of spectral filters on energy conversion, but there is a lack of comprehensive simulation-based analyses that quantify how spectral splitting specifically affects the effi-ciency of both the PV and thermal components. Additionally, few studies have looked at how the properties of spectral filters, environmental conditions, and system design parame- ters interact.

This paper aims to address these gaps by designing a CPVT system that integrates a spectral filter and evaluating its performance through simulations. Specifically, the effects of spectral splitting on PV cell efficiency and the overall energy output of the system under various conditions are explored. The results provide valuable insights into optimizing CPVT systems and demonstrate the potential of spectral splitting as a transformative technology for enhanced solar energy utilization.

2. Methodology

2.1. System design

The CPVT system in this study used commercial photovoltaic and thermal components, which requires a redesign of previous systems. The system layout is illustrated in figure 1, where a heliostat reflector, composed of flat mirrors, directs concentrated solar radiation onto the PV module. A dual-axis tracking system ensures optimal solar energy collection by adjusting to the sun’s movement. This design differs from conventional heliostat systems, which typically use multi-row single-axis tracking reflectors mounted on flat ground.

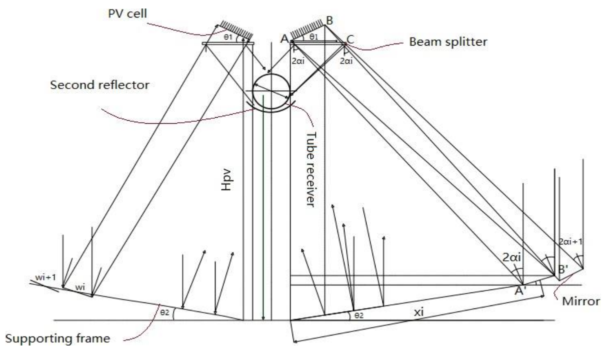

Figure 1: Sketch of the concentrating system.

To enhance system efficiency, the mirrors are placed at an inclined angle, minimizing horizontal gaps, reducing shadowing effects, and improving light distribution. The mirrors focus solar radiation onto a spectral filter positioned between the PV module and the thermal receiver. This filter separates the solar spectrum into two bands: high-energy photons directed toward the PV module and lower-energy photons absorbed by the thermal receiver.

The spectral filter used in this study is a $Nb_2O_5/SiO_2/K9$ filter, developed in our previous work, with a transmittance of 87.56% in photovoltaic pass-band [22]. This filter plays an important role in splitting the solar spectrum, directing high-energy photons to the PV module and low-energy photons to the thermal collector, ensuring optimal energy conversion.

A key aspect of the concentrator’s design is the arrangement of the mirrors to optimize light concentration. The length (w_i) and inclination angle (α_i) of the i-th mirror relative to the horizontal plane are defined in relation to the photovoltaic panel’s length (L) and inclination angle (θ_1) by the following equation:

$$\omega_i(\cos\alpha_i+\sin\alpha_i\cdot\tan 2\alpha_i) =L(\cos\theta_1+\sin\theta_1\cdot\tan 2\alpha_i) \quad (1)$$

where ω_i is the width of the i-th mirror, α_i is the inclination angle of the i-th mirror, L is the length of the photovoltaic panel, θ_1 is the inclination angle of the photovoltaic panel. The installation positions (x_i) and angles (α_i) of the mirrors are determined using geo- metric relationships. The positioning of the mirrors is derived to ensure that incident solar radiation is effectively reflected onto the PV module while maintaining structural integrity. The relationship governing these parameters is given by:

$$\tan 2\alpha_i\cdot(H_{pv}-x_i\cdot\sin\theta_2+b_i\cdot\sin\alpha_i) =x_i\cdot\cos\theta_2-b_i\cdot\cos\alpha_i) \quad (2)$$

where H_{pv} is the height of the photovoltaic panel, x_i is the horizontal position of the i-th mirror, θ_2 is the tilt angle of the receiver, b_i is the spacing between mirrors.

$$0.5(\cos\theta_1+\sin\theta_1.\tan 2\alpha_i) =x_i(\cos\theta_2+\sin\theta_2\cdot\tan 2\alpha_i)-H_{pv}\cdot\tan 2\alpha_i \quad (3)$$

To prevent misalignment and ensure light concentration, the positioning of each mirror relative to the next is constrained by:

$$x_i.\cos\theta_2+(\omega_i+b_i).\cos\alpha_i =x_{i+1}.\cos\theta_2-b_{i+1}.\cos\alpha_{i+1} \quad (4)$$

where x_{i+1}, b_{i+1}, and α_{i+1} correspond to the next mirror in the sequence.

The geometric concentration ratio (CR) is an important parameter for evaluating system performance. It represents the ratio of the total reflective surface area (A_1) to the receiver aperture area (A_2):

$$CR=\frac{A_1}{A_2}=\frac{1}{L}\sum_{i=1}^{n}\omega_i.\cos\alpha_i \quad (5)$$

where A_1 is the total reflective surface area, A_2 is the receiver aperture area, and n is the total number of mirrors.

In addition, the aperture utilization ratio (γ) is introduced to measure the efficiency of the use of the concentrator aperture area:

$$\gamma=\frac{\sum_{i=1}^{n}\omega_i.\cos\alpha_i}{x_n.\cos\theta_2+(\omega_n+b_n).\cos\alpha_n} \quad (6)$$

where x_n, w_n, and b_n refer to the last mirror in the arrangement.

To clarify the influence of the tilt angles θ_1 (PV module) and θ_2 (support structure) on the geometric concentration ratio (CR) and the aperture utilization ratio (γ), a parametric analysis was carried out. Based on the geometric relations established from Equations (1) to (6), different scenarios were defined to evaluate system performance and determine the optimal configuration.

First, to study the effect of θ_1 on the system, θ_2 was fixed at 15°, while θ_1 was varied among 0°, 15°, 30°, and 45°. As shown in figure 2, the concentration ratio *CR* exhibits low sensitivity to variations in θ_1, indicating that changes in the PV tilt angle have limited impact on the system's ability to concentrate sunlight. In contrast, the aperture utilization ratio γ reaches its maximum at θ_1 = 45°, suggesting that this tilt angle provides optimal use of the aperture area by balancing concentrated light collection and effective PV surface coverage.

These equations guide the optimal design of the concentrating system, ensuring efficient light distribution and maximizing energy conversion. The use of a spectral filter further enhances performance by directing photons to their most suitable energy conversion pathways, thereby improving overall system efficiency.

2.2. Simulation

The simulation assumed that the total received power was treated uniformly throughout the system, with solar irradiance modeled according to the AM1.5 standards. The intensity of solar radiation at ground level was assumed to be uniform, and the solar irradiance was treated as a plane wave near the system.

For the simulation, a PERC monocrystalline PV cell was selected, with an open-circuit voltage of 0.655 V, a short-circuit current of 39.7 mA/cm², and a fill factor of 0.794, according to PV Lighthouse data. The thermal receiver, obtained from the National Center for Quality Supervision and Testing of Solar Heating Systems (Beijing), had an efficiency of 56% at 80°C and a heat loss coefficient of 0.56 W/(m²·°C). The simulation was conducted using AM1.5 solar irradiance.

The photovoltaic efficiency, denoted as ηpv, is calculated by integrating the wavelength-dependent conversion efficiency normalized by the energy received by the heliostat:

$$\eta_{pv} = \frac{\int \eta_{pv}(\lambda) d\lambda}{Q_{heliostat}} \quad (7)$$

where:

- ηpv(λ): Conversion efficiency of the PV cell at wavelength λ;
- Qheliostat: Total solar energy received by the heliostat mirrors.

The absorbed thermal power of the receiver is given by:

$$\text{Qabsorbed} = \alpha \cdot \text{Qthermal} \quad (8)$$

where:

- α = 0.91: Absorptance of the thermal receiver;
- Qthermal: Solar energy incident on the thermal component.

The net thermal energy is:

$$\text{Qthermal,net} = \text{Qabsorbed} - \text{Qloss} \quad (9)$$

The total heat loss consists of convective and radiative components:

$$\text{Qloss} = \text{Qconv} + \text{Qrad} \quad (10)$$

$$\text{Qconv} = \text{hconv} \cdot \text{Aaperture} \cdot (\text{Tthermal} - \text{Tamb}) \quad (11)$$

$$Q_{rad} = \varepsilon.\sigma.A_{aperture}.(T_{thermal}^4 - T_{amb}^4) \quad (12)$$

with:

h_{conv} = 10 W/(m^2 · K): Convective heat transfer coefficient;

- *ε = 0.056: Emissivity of the receiver surface;*
- *σ: Stefan–Boltzmann constant;*
- *Tthermal, Tamb: Receiver surface and ambient temperature;*
- *Aaperture: Aperture area of the thermal receiver.*

The thermal efficiency is calculated as:

$$\eta\text{thermal,elec} = \frac{\text{Qthermal,net}}{\text{Qheliostat}} \quad (13)$$

Assuming a thermal-to-electric conversion efficiency ηthermal-elec = 25% using a Rankine cycle [23], the corresponding electrical output is:

$$\text{Pthermal,elec} = \text{Qthermal,net} \cdot \eta\text{thermal,elec} \quad (14)$$

Thus, the thermal-to-electrical efficiency becomes:

$$\eta\text{thermal,elec} = \frac{\text{Pthermal,elec}}{\text{Qheliostat}} \quad (15)$$

To enable a quantitative performance analysis of the system, a high-precision ray-tracing-based optical simulation method was employed. This approach tracks each individual light ray as it propagates through different media and structural surfaces, accurately capturing the transport path and energy distribution of solar radiation within the system. Based on this, a complete three-dimensional structural model was developed to simulate, in detail, the transmission, refraction, reflection, and absorption of the solar spectrum between the photovoltaic and thermal components. This modeling provided reliable data support for subsequent efficiency calculations and energy flux evaluations.

The system model included planar heliostats, a spectral-splitting filter, a thermal receiver, a PV module, a secondary reflector, and incident solar rays. All geometric dimensions and positional parameters were defined based on the structural configuration introduced earlier. During simulation, the incident solar spectrum followed the AM1.5 standard, and the rays were assumed to be perpendicularly incident to simplify the analysis.

A total of 106 rays were traced to ensure convergence of the computation. Optical properties of the materials (e.g., refractive index, absorptance) were modeled based on experimentally measured spectral characteristics and interpolated within the 300–2500 nm wavelength range to capture spectral-dependent behavior accurately. This ensured high spectral resolution and realistic modeling of solar energy conversion under full-spectrum irradiation. Output parameters included the radiative flux distribution on each component surface and the effective spectral power reaching the photovoltaic cell. To improve computational efficiency, geometric symmetry was exploited, and only half of the system's cross-section was modeled where applicable.

3. Result and discussion

3.1. Design results

The effect of the PV tilt angle (θ1) on the concentration ratio and aperture utilization ratio was evaluated, with the results shown in figure 2. The concentration ratio exhibited minimal sensitivity to changes in the tilt angle, indicating that the tilt angle did not significantly impact the system's ability to concentrate sunlight. However, the aperture utilization ratio reached its maximum value when the PV tilt angle was approximately 45°. This suggests that a tilt angle of 45° optimized the use of the aperture area, balancing sunlight concentration and the effective coverage of the photovoltaic device.

Next, the impact of the support structure angle (θ2) on the system's performance was investigated, as shown in figure 3. As the concentrator width (xi) increased, the aperture utilization ratio initially rose sharply due to the effect of the fixed shading area of the PV device. After reaching a maximum, the ratio began to decrease as the horizontal gaps between adjacent mirrors widened. A minor jump in aperture utilization occurred when θ2 exceeded 20°, resulting from the discrete geometric alignment of the mirrors. This variation has a negligible impact on system performance. When θ2 was increased beyond 20°, the aperture utilization ratios tended to converge for different values of xi, while the concentration ratios increased as θ2 decreased. Both parameters stabilized when θ2 was reduced to 20°. Therefore, the optimal angle for the support structure was determined to be approximately 20°, maximizing both concentration and aperture utilization.

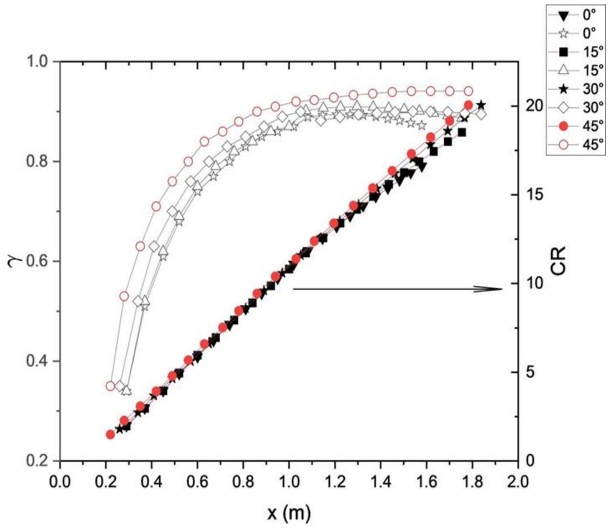

Figure 2: Relationships of the concentration ratio CR and the aperture utilization ratio *γ* with the concen- trator width x_i at different PV tilt angle θ_1 (where θ_2 = 15°, *L* = 80 mm, and H_{pv} = 1.5 m).

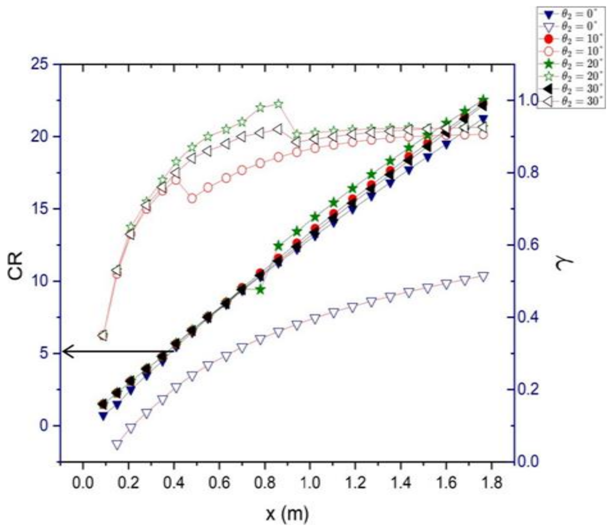

Figure 3: Relationships of the concentration ratio CR and the aperture utilization ratio *γ* with the concentra- tor width x_i at different angle of the support structure (θ_2) (where θ_1 = 45°, *L* = 80 mm, and H_{PV} = 1.5 m).

The number of reflective mirrors (*i*), their installation positions (x_i), and installation angles (α_i) were determined using formulas (1) to (6), with the optimal values of $\theta_1 = 45^{\circ}$ and $\theta_2 = 20^{\circ}$. The configuration consisted of 23 mirrors on each side, due to the symmetry of the system. The concentration ratio (CR) was obtained to be 20. The results, summarized in Table 1, show that the mirror tilt angles (α_i) steadily increased with x_i, while the mirror widths (ω_i) initially grew before slightly decreasing as x_i continued to increase. A small fluctuation in mirror width between mirrors 5 and 6 results from the geometric relationship between tilt angle and spacing. This deviation (less than 0.003 m) remains within the optical design tolerance and has no noticeable influence on the concentration ratio or the system optimization.

This setup plays a key role in maximizing the system's efficiency by ensuring optimal alignment of mirrors for effective sunlight concentration. Now, the impact of these configurations on the system's performance will be explored in the following simulation section.

Table 1: Results for the number, installation positions, and angles of the mirrors using the optimal $\theta_1 = 45^{\circ}$ and θ2 = 20°.

Mirror No. i	1	2	3	4	5	6	7	8
Position x (m)	0.091	0.15	0.22	0.28	0.35	0.42	0.49	0.56
Tilt angle α ($^{\circ}$)	1.1	2.249	3.446	4.696	5.997	7.347	8.743	10.178
Mirror width ω (m)	0.059	0.061	0.063	0.065	0.067	0.070	0.072	0.074
Mirror No. i	**9**	**10**	**11**	**12**	**13**	**14**	**15**	**16**
Position x (m)	0.63	0.71	0.78	0.86	0.94	1.03	1.110	1.195
Tilt angle α ($^{\circ}$)	11.648	13.144	14.660	16.185	17.713	19.232	20.736	22.185
Mirror width w (m)	0.076	0.078	0.080	0.081	0.083	0.084	0.085	0.086
Mirror No. i	**17**	**18**	**19**	**20**	**21**	**22**	**23**	
Position x (m)	1.281	1.365	1.450	1.534	1.618	1.701	1.783	
Tilt angle α ($^{\circ}$)	23.571	24.889	26.137	27.314	28.420	29.458	30.430	
Mirror width ω (m)	0.087	0.088	0.088	0.089	0.089	0.089	0.089	

3.2. Simulation results

The simulation was conducted to evaluate the performance of two configurations: a standalone photovoltaic (PV) system and a hybrid system incorporating a spectral filter and a secondary reflector. These configurations are illustrated in figure 4. The analysis was performed on one half of the symmetric system, with the irradiance set to 800 W/m², as detailed in the methodology section.

In the hybrid system, the spectral filter receives 38.146 W, demonstrating the effectiveness of the reflection mirrors in directing sunlight to the solar components. This efficient reflection ensures optimal energy distribution between the photovoltaic and thermal receivers, thereby enhancing overall system performance. Figure 5 shows the energy distribution received by the spectral filter, highlighting its ability to direct photons to their respective receivers while maintaining high system efficiency.

The energy transmitted to the photovoltaic cells in the hybrid system is further illustrated in figure 6. The orange-shaded area in the spectrum represents the transmitted energy directed to PV cells, primarily within the 580–1100 nm wavelength range, which is ideal for photovoltaic conversion. This demonstrates the efficiency of the spectral filter in enabling optimal energy utilization for electricity generation.

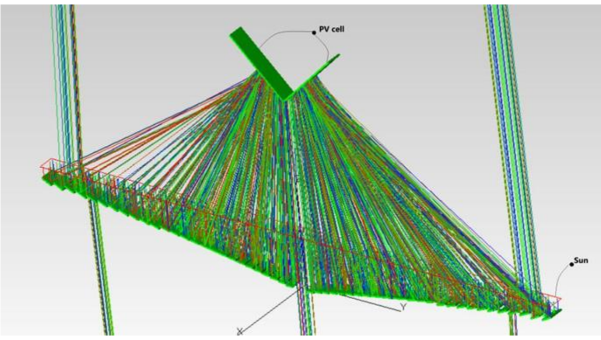

a) standalone PV system flux distribution

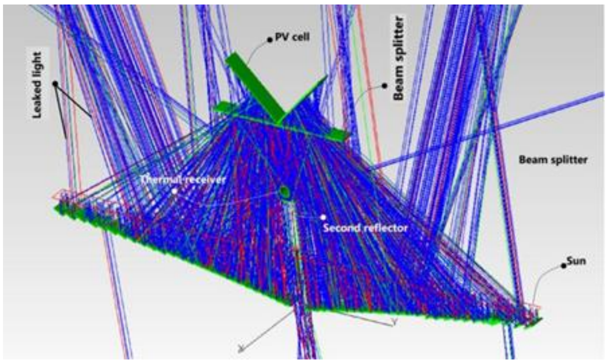

b) Flux distribution in the hybrid system.

Figure 4: Simulated configurations of (a) standalone PV system and (b) hybrid system.

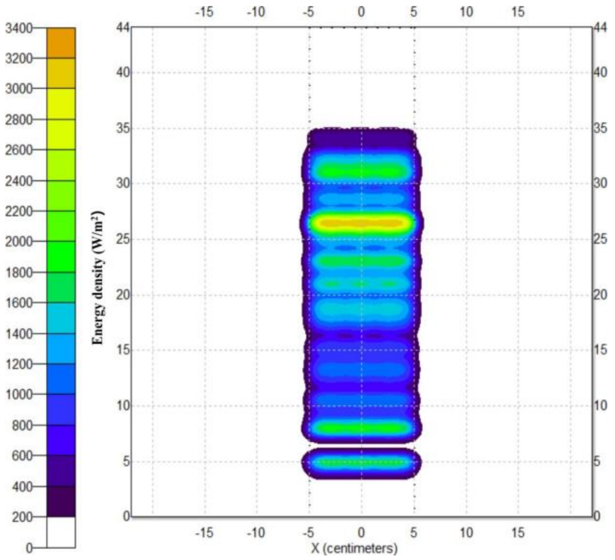

Figure 5: Energy received by the spectral filter in the hybrid system.

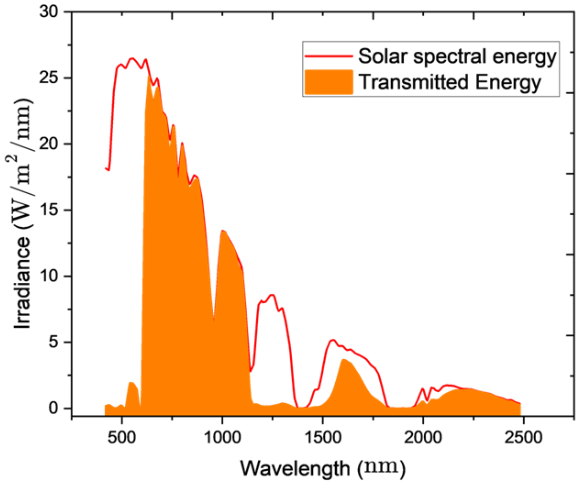

Figure 6: Spectral energy transmitted to the PV cells in the hybrid system.

The flux distribution on the thermal receiver, as shown in figure 7a, demonstrates a relatively uniform spread across its surface. This result is further enhanced by the contribution of the second reflector, which redirects light that would otherwise be lost from the primary concentrator back to the thermal receiver. The total flux on the thermal receiver is 15.558 W, indicating that the second reflector significantly improves thermal energy absorption. Without the second reflector, much of this energy would be lost, resulting in lower thermal efficiency. By effectively capturing scattered or missed light, the second reflector ensures maximum utilization of the available energy.

The inclusion of the second reflector not only improves thermal energy collection but also minimizes energy losses, as shown in figure 7b. The second reflector plays a crucial role in capturing light that would otherwise escape and redirecting it back to the thermal receiver. This enhanced light management further increases the thermal energy production efficiency of the hybrid system.

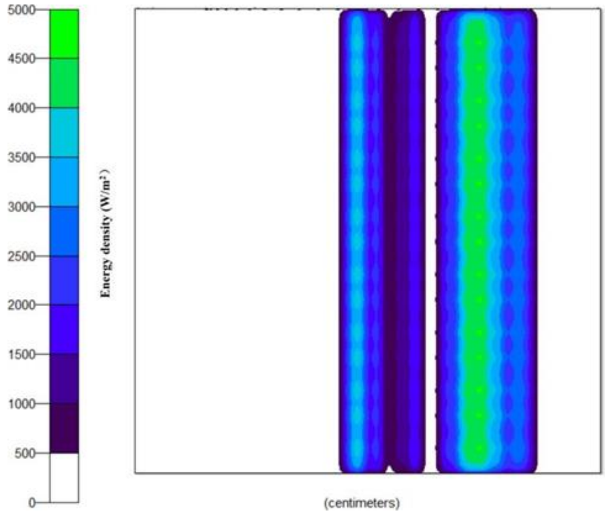

a) Flux distribution on the thermal tube receiver in the hybrid system.

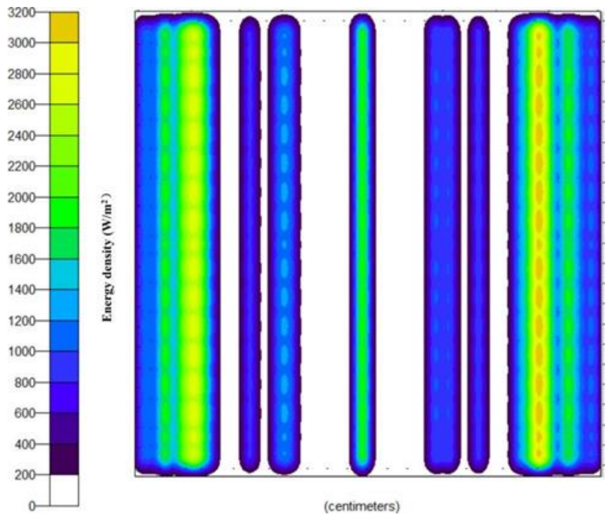

b) Flux distribution on the second reflector in the hybrid sys- tem.

Figure 7: Flux profiles on the thermal receiver and second reflector in the hybrid system.

Compared to the standard PV system, the hybrid system demonstrates superior performance over the standalone PV system. In the standalone system, PV cells absorb a broad spectrum of sunlight, including suboptimal wavelengths for silicon-based photovoltaic conversion, resulting in inefficient energy utilization. Conversely, the hybrid system, by incorporating the spectral filter and secondary reflector, effectively separates high-energy and low-energy photons, directing them to the appropriate receivers. Figure 8 illustrates the flux profiles for both configurations, emphasizing the efficiency advantage of the hybrid system. Both configurations, highlighting the efficiency advantage of the hybrid system.

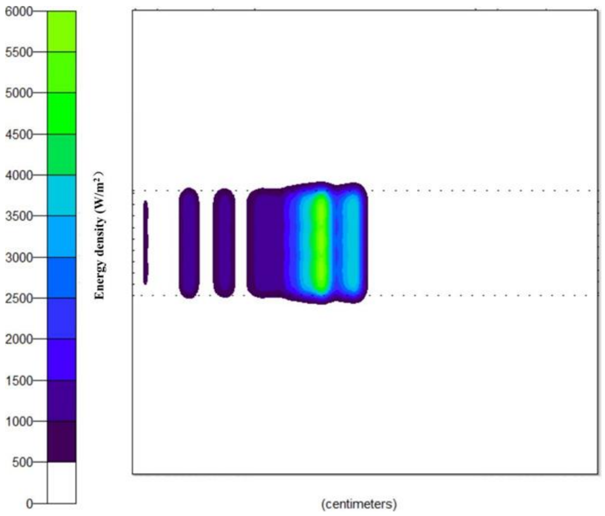

a) Standalone system

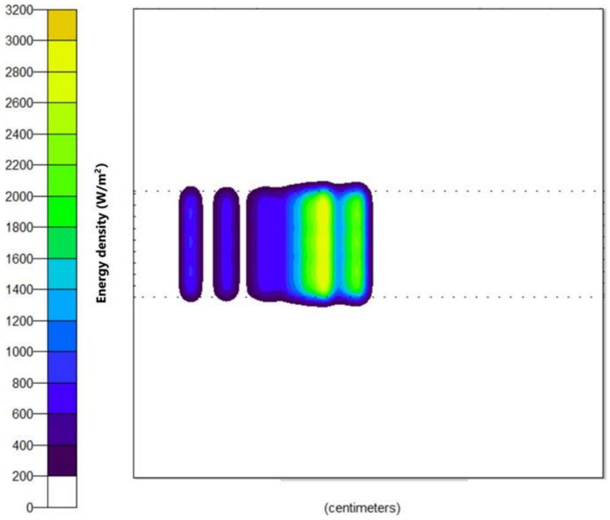

b) Hybrid system

Figure 8. Flux on PV cells in the (a) standalone system and (b) hybrid system.

The performance of the standalone monocrystalline PV system, proposed hybrid system, P. Hu hybrid system, and Hongxu Du's CPVT system are compared in Table 2. Key metrics include the electrical efficiency of the PV cells, the thermal efficiency of the thermal receiver, and the overall energy utilization efficiency.

The results in Table 2 highlight the performance of the proposed hybrid CPVT system.

The proposed hybrid CPVT system achieves an overall electrical efficiency of 18.00%, surpassing Du's system (15.05%) and P. Hu's system (11.99%). This improvement mainly results from the advanced spectral beam-splitting filter that enables more efficient utilization of high-energy photons for photovoltaic conversion and from the optimized concentrator geometry that enhances flux density on the PV module without inducing excessive thermal stress. Compared with previous configurations, the proposed design minimizes optical mismatch losses by precisely separating the solar spectrum into high- and low-energy bands, ensuring that high-energy photons are fully utilized for power generation while reducing thermal loading on the PV cell.

In terms of thermal efficiency, Du's system attains 49.8%, while the proposed system and P. Hu's system reach 34.29% and 30.00%, respectively. Although Du's design yields a higher thermal fraction, this gain comes at the expense of electrical output, as its configuration prioritizes heat recovery from low-energy photons. This trade-off highlights that higher thermal efficiency does not necessarily translate to superior overall energy utilization, especially when the goal is to maximize high-grade electrical output.

The key advantage of the proposed system lies in the quality and usability of the generated energy. While most conventional CPVT systems emphasize heat recovery, the present configuration is designed to maximize solar exergy conversion into electricity, thereby enhancing system-level energy quality. Unlike conventional CPVT configurations that focus on heat recovery, the present design converts a greater share of solar exergy into high-grade electrical energy, which can be directly used or stored with minimal loss. This higher proportion of high-grade output indicates better overall exergy efficiency, providing greater flexibility for grid integration or hybrid renewable systems. This balance between electrical and thermal performance demonstrates a more optimal utilization of the solar spectrum. Consequently, even with moderately lower thermal efficiency, the proposed hybrid CPVT system delivers superior overall energy quality and conversion value, underscoring its competitiveness for high-efficiency solar power applications and establishing a clear advantage over existing CPVT designs.

Table 2: Performance metrics of standalone, proposed hybrid, previous research systems, and Hongxu Du's system.

Metric(%)	Stand alone PV	Proposed CPVT	P.Hu [24]	Hongxu Du [25]
PV electrical efficiency	23.83	18.00	11.99	15.05
Thermal efficiency	–	34.29	30.00	49.8
Overall electrical efficiency	23.83	26.57	–	–

Although this research focuses on monocrystalline systems, the proposed optimization strategies can also be applied to polycrystalline hybrid systems (PHS). By adapting key parameters such as concentrator configuration and spectral filter characteristics, similar im- provements in energy efficiency and system performance could be achieved for PHS, helping to address their inherent efficiency challenges.

To further evaluate the robustness of the proposed system, a sensitivity analysis was conducted with respect to Direct Normal Irradiance (DNI). Other environmental factors such as wind speed, ambient temperature, and seasonal variation were not considered here, as the main objective was to isolate the optical–thermal coupling effects under controlled solar conditions. As shown in Fig. 9, the electrical efficiency (ηpv) slightly decreases with increasing DNI, which is attributed to the temperature rise of the photovoltaic cells under higher irradiance, leading to a reduction in open-circuit voltage. In contrast, the thermal efficiency (ηthermal) increases due to enhanced solar absorption at the receiver surface. Overall, the total system performance remains relatively stable, demonstrating that the proposed hybrid CPVT configuration maintains high operational reliability under fluctuating solar intensities.

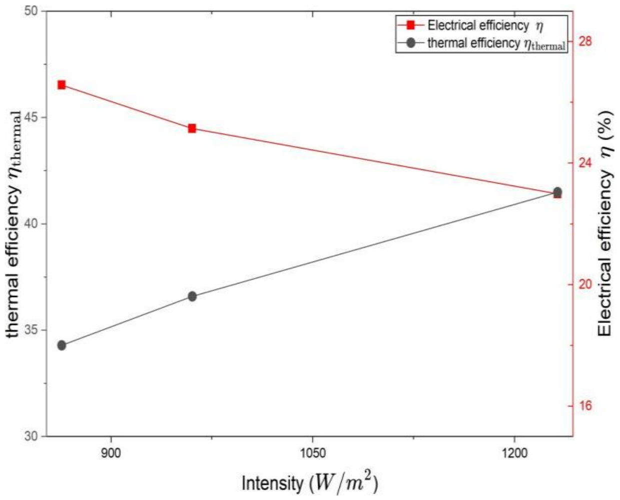

Figure 9: Sensitivity of the electrical (η_{pv}) and thermal ($\eta_{thermal}$) efficiencies of the proposed CPVT system under varying Direct Normal Irradiance (DNI). The electrical efficiency decreases slightly with DNI due to PV temperature rise, while the thermal efficiency increases as a result of improved solar absorption.

4. Conclusion

The integration of spectral splitting directs high-energy and low-energy photons to the photovoltaic and thermal components, respectively, thereby improving overall energy utilization. The results indicate that optimizing the tilt angles of the photovoltaic and support structures is crucial for maximizing aperture utilization and enhancing the concentration ratio.

The inclusion of a secondary reflector enhances thermal energy absorption by reducing energy losses, contributing to better thermal performance.

The study highlights the potential benefits of spectral beam splitting and secondary reflectors in improving solar energy conversion in hybrid CPVT systems, suggesting that further optimization could enhance solar energy utilization in high-efficiency applications, particularly for generating high-quality electrical output.

5. Acknowledgements

This work was supported by the Program of Beijing Huairou Laboratory (ZD2023008A).

6. Funding sources

This research did not receive any specific grant from funding agencies in the public, commercial, or not-for-profit sectors.

7. References

[1] T. Kober, H.-W. Schiffer, M. Densing, and E. Panos. Global energy perspectives to 2060 – wec's world energy scenarios 2019. Energy Strategy Reviews, 31:100523, 2020.

[2] Sven Rühle. Tabulated values of the shockley–queisser limit for single junction solar cells. Solar Energy, 130:139–147, 2016.

[3] Ugo Pelay, Lingai Luo, Yilin Fan, Driss Stitou, and Mark Rood. Thermal energy storage systems for concentrated solar power plants. Renewable and Sustainable Energy Reviews, 79:82–100, 2017.

[4] Omar Ellabban, Haitham Abu-Rub, and Frede Blaabjerg. Renewable energy resources: Current status, future prospects and their enabling technology. Renewable and Sustain-able Energy Reviews, 39:748–764, 2014.

[5] T.T. Chow. A review on photovoltaic/thermal hybrid solar technology. Applied Energy, 87(2):365–379, 2010.

[6] Xing Ju, Zhifeng Wang, Gilles Flamant, Peng Li, and Wenyu Zhao. Numerical analy-sis and optimization of a spectrum splitting concentration photovoltaic–thermoelectric hybrid system. Solar Energy, 86(6):1941–1954, 2012.

[7] D. Costa, S. De Regel, G. Espadas-Aldana, H. Laget, R. Kishore, Y. Meuret, and

F. Duerinckx. Environmental and economic impacts of photovoltaic integration in con-centrated solar power plants. Solar Energy, 274:112550, 2024.

[8] Greg Ingersoll and James Leger. Optimization of multi-grating volume holographic spectrum splitters for photovoltaic applications. Applied Optics, 55:5399, 07 2016.

[9] Chien-Jen Tang, Cheng-Chung Jaing, Kuan-Shiang Lee, and Cheng-Chung Lee. Resid-ual stress in ta2o5-sio2 composite thin-film rugate filters prepared by radio frequency ion-beam sputtering. Appl. Opt., 47(13):C167–C171, May 2008.

[10] Charles E. Keffer, Marsha R. Torr, Muamer Zukic, James F. Spann, Douglas G. Torr, and Jongmin Kim. Radiation damage effects in far-ultraviolet filters, thin films, and substrates. Appl. Opt., 33(25):6041–6045, Sep 1994.

[11] Yu Gao, Xiaoxiao Yang, Xingyuan Yang, Yanguo Zhang, Hui Zhou, and Qinghai Li. Effects of beam splitting on photovoltaic properties of monocrystalline silicon, mul-ticrystalline silicon, gaas, and perovskite solar cells for hybrid utilization. International Journal of Green Energy, 20:1–9, 09 2022.

[12] Xing Ju, Chao Xu, Xue Han, Xiaoze Du, Gaosheng Wei, and Yongping Yang. A review of the concentrated photovoltaic/thermal (cpvt) hybrid solar systems based on the spectral beam splitting technology. Applied Energy, 187:534–563, 2017.

[13] V.V. Tyagi, S.C. Kaushik, and S.K. Tyagi. Advancement in solar photovoltaic/thermal (pv/t) hybrid collector technology. Renewable and Sustainable Energy Reviews, 16(3):1383–1398, 2012.

[14] P.G. Charalambous, G.G. Maidment, S.A. Kalogirou, and K. Yiakoumetti. Photovoltaic thermal (pv/t) collectors: A review. Applied Thermal Engineering, 27(2):275–286, 2007.

[15] A.G. Imenes, D. Buie, D.R. Mills, P. Schramek, and S.G. Bosi. A new strategy for improved spectral performance in solar power plants. Solar Energy, 80(10):1263–1269, 2006. Solar Power and Chemical Energy Systems (SolarPACES'04).

[16] Felipe Crisostomo, Robert A. Taylor, Desiree Surjadi, Ahmad Mojiri, Gary Rosengarten, and Evatt R. Hawkes. Spectral splitting strategy and optical model for the development of a concentrating hybrid pv/t collector. Applied Energy, 141:238–246, 2015.

[17] A.G. Imenes, D. Buie, and D. McKenzie. The design of broadband, wide-angle inter-ference filters for solar concentrating systems. Solar Energy Materials and Solar Cells, 90(11):1579–1606, 2006.

[18] Gang Wang, Xiao-Fang Cheng, Peng Hu, Ze-Shao Chen, Yang Liu, and Lei Jia. The-oretical analysis of spectral selective transmission coatings for solar energy pv system. International Journal of Thermophysics, 34, 12 2011.

[19] Gang Wang, Botong Wang, Yubo Yao, Jianqing Lin, Zeshao Chen, and Peng Hu. Para-metric study on thermodynamic performance of a novel pv panel and thermal hybrid solar system. Applied Thermal Engineering, 180:115807, 2020.

[20] Huaxu Liang, Fuqiang Wang, Luwei Yang, Ziming Cheng, Yong Shuai, and Heping Tan. Progress in full spectrum solar energy utilization by spectral beam splitting hybrid pv/t system. Renewable and Sustainable Energy Reviews, 141:110785, 2021.

[21] Jeeja Jacob, A.K. Pandey, Nasrudin Abd Rahim, Jeyraj Selvaraj, M. Samykano,

R. Saidur, and V.V. Tyagi. Concentrated photovoltaic thermal (cpvt) systems: Recent advancements in clean energy applications, thermal management and storage. Journal of Energy Storage, 45:103369, 2022.

[22] Abdallah Bourhani Said, Lei Tang, Hui Zhou, Yanguo Zhang, and Qinghai Li. Investi-gation of nb2o5/sio2 short-wave pass filters for beam-splitting application in a pv/csp solar hybrid system. Appl. Opt., 64(5):1196–1205, Feb 2025.

[23] J. Siviter, A. Montecucco, and A.R. Knox. Rankine cycle efficiency gain using thermo-electric heat pumps. Applied Energy, 140:161–170, 2015.

[24] Peng Hu, Qian Zhang, Yang Liu, ChunChen Sheng, XiaoFang Cheng, and ZeShao Chen. Optical analysis of a hybrid solar concentrating photovoltaic/thermal (cpv/t) system with beam splitting technique. Science China Technological Sciences, 56(6):1387–1394, Jun 2013.

[25] Hongxu Du, Longyu Xia, Gaosheng Wei, Gang Wang, and Xiaoze Du. Study on a novel solar spectral beam splitting photovoltaic/thermal system based on secondary reflection. Energy, page 134837, 2025.